Materials Research Letters

ISSN: (Print) 2166-3831 (Online) Journal homepage: https://www.tandfonline.com/loi/tmrl20

Synthesis of surfactant-free Cu–Pt dendritic heterostructures with highly electrocatalytic performance for methanol oxidation reaction

Shendong Kang, Guanhui Gao, Xiaobin Xie, Tamaki Shibayama, Yanhua Lei, Yan Wang & Lintao Cai

To cite this article: Shendong Kang, Guanhui Gao, Xiaobin Xie, Tamaki Shibayama, Yanhua Lei, Yan Wang & Lintao Cai (2016) Synthesis of surfactant-free Cu–Pt dendritic heterostructures with highly electrocatalytic performance for methanol oxidation reaction, Materials Research Letters, 4:4, 212-218, DOI: 10.1080/21663831.2016.1179228

To link to this article: https://doi.org/10.1080/21663831.2016.1179228

MATER. RES. LETT., 2016
VOL. 4, NO. 4, 212–218
http://dx.doi.org/10.1080/21663831.2016.1179228

MATERIALS RESEARCH LETTERS
Taylor & Francis
Taylor & Francis Group

Synthesis of surfactant-free Cu–Pt dendritic heterostructures with highly electrocatalytic performance for methanol oxidation reaction

Shendong Kang[a,b], Guanhui Gao[a,c], Xiaobin Xie[d], Tamaki Shibayama[e], Yanhua Lei[e], Yan Wang[b] and Lintao Cai[a]

[a]Guangdong Key Laboratory of Nanomedicine, CAS Key Laboratory of Health Informatics, Shenzhen Institutes of Advanced Technology, Chinese Academy of Science, Shenzhen, People's Republic of China; [b]Nano Science and Technology Institute, University of Science & Technology of China, Suzhou, People's Republic of China; [c]Paul-Drude-Institut für Festkörperelektronik, Berlin, Germany; [d]Debye Institute for Nanomaterials science, Utrecht University, Utrecht, The Netherlands; [e]Center for Advanced Research of Energy and Materials, Faculty of Engineering, Hokkaido University, Hokkaido, Japan

ABSTRACT

A facile and free surfactant strategy is explored to synthesize Cu–Pt bimetallic nano-heterostructures with dendritic exterior. For comparison, the Cu–Pt coral-like nanoparticles are fabricated by using CTAC as a surfactant. The well-designed Cu–Pt dendritic spherical heterostructures exhibit superior enhanced electrocatalytic activity and stability toward methanol oxidation reaction in alkaline media, compared to the Cu–Pt coral-like nanoparticles and the commercial Pt/C, respectively. The advanced technique for fabricating Cu–Pt dendritic spherical heterostructures could pave a way to pursue low-cost Pt-based catalysts, maintaining highly promoted electrocatalytic performance and durability.

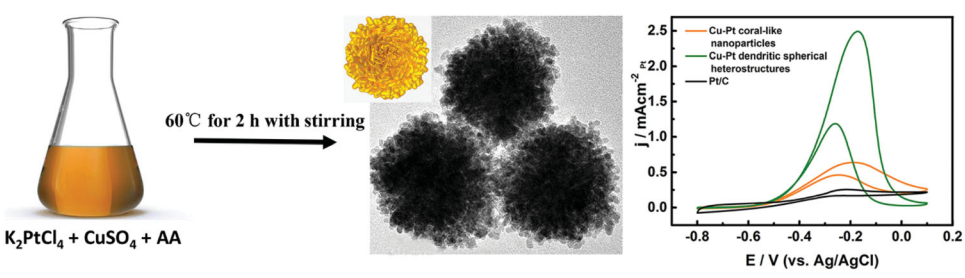

ARTICLE HISTORY
Received 11 March 2016
Accepted 12 April 2016

KEYWORDS
Cu–Pt dendritic spherical heterostructures; Cu–Pt coral-like nanoparticles; electrocatalytic property; methanol oxidation reaction

IMPACT STATEMENT

The well-designed Cu–Pt dendritic spherical heterostructures are synthesized without any surfactant, which demonstrate highly promoted electrocatalytic performance and durability toward methanol oxidation reaction.

Introduction

Very recently, metallic nano-heterostructures with distinctive architecture and size have been motivated to tailor catalytic performance and thermal stability for achieving more potential applications such as oxygen reduction,[1–3] methanol oxidation[4,5] and formic acid oxidation.[6] Considerable attention has been focused on platinum (Pt)-based nanostructures with various morphologies, which could be applied for electrocatalytic methanol oxidation reaction (MOR) because of its slow kinetics and the demand for fuel-cell cathodes. [7–9] The promoted catalytic activity is usually explained and influenced by synergistic effect,[10] bifunctional mechanism and electronic effects (include lattice strain effects, surface ligand effects and geometric effects).[11–14] Notably, the morphology plays a significant role in determining the selectivity and active sites. Plenty of Pt-based nano-architectures with typical shape and size have been successfully synthesized, exhibiting high catalytic activity.[15–17] Such as Pt cubes, tetrahedrons, truncated

CONTACT Lintao Cai lt.cai@siat.ac.cn; Guanhui Gao gao@pdi-berlin.de
A more detailed information on experiments is available at 10.1080/21663831.2016.1179228.

Supplemental data for this article can be accessed here. http://dx.doi.org/10.1080/21663831.2016.1179228

octahedrons, single-crystal Pt nanowires and Pt nanoalloys covered by high-index facets.[18–23] Numerous examples of adatoms to Pt have been conducted including Ru,[24,25] Co,[26] Cu[5,27,28] and Pd.[29] Recently, our group developed a facile strategy to synthesize well-designed Au/Ag/Pt trimetallic heterogeneous nanocrystals with highly effective catalytic properties and stability.[30]

In conventional wet chemical methods, the surfactants are frequently used in colloidal synthesis to inhibit nanoparticles extreme overgrowth and aggregation, as well as to control the structural characteristics of the resulted nanoparticles in a precise manner. However, these surfactants such as polyvinylpyrrolidone (PVP) could occupy surface activity sites due to their strong adsorption, which would be difficult to be removed, dramatically declining the catalytic activity of nanoparticles.[31] Therefore, it is essential to develop high techniques for synthesis of green and distinctive morphological Pt-based nanostructures without any surfactant.[32]

Herein, we engage in exploiting facial and universal techniques to synthesize Cu–Pt bimetallic nanoheterostructures with dendritic morphology. As expected, the well-designed Cu–Pt dendritic spherical heterostructures exhibit superior electrocatalytic functions. Simply, the Cu–Pt dendritic spherical heterostructures are synthesized via a one-step wet chemical strategy, by simultaneous reduction of potassium tetrachloroplatinate (II) (K_2PtCl_4) and copper sulfate ($CuSO_4$) with 3:1 molar ratio in ultrapure water as solvent at 60°C for 2 h, l-ascorbic acid (AA) as the reducing agent. Neither surfactants nor dispersion agents are introduced in the above fabrication process. For comparison, Cu–Pt coral-like nanoparticles are synthesized with highly uniform size and morphology, using cetyl trimethyl ammonium chloride (CTAC) as a surfactant. The schematic procedures of Cu–Pt dendritic spherical heterostructures and Cu–Pt coral-like nanoparticles are shown in Figure 1. Several experimental parameters on growth of Cu–Pt alloys are investigated through systematic orthogonal methods. The Cu–Pt dendritic spherical heterostructures exhibit highly promoted electrochemical activity and durability for MOR in alkaline media compared to Cu–Pt coral-like nanoparticles and commercial Pt/C, respectively.

Experimental

Chemicals and materials

Potassium tetrachloroplatinate (II) (K_2PtCl_4, 99.95%, J&K Scientific), copper sulfate ($CuSO_4$), l-Ascorbic acid (AA, 99%, J&K Scientific), cetyl trimethyl ammonium chloride (CTAC, 99%, J&K Scientific), potassium hydride (KOH, ≥ 85.0%, Shanghai Lingfeng Chemical Reagent Co. Ltd.), methanol (≥ 99.5%, Shanghai Lingfeng Chemical Reagent Co. Ltd.), Nafion® perfluorinated resin

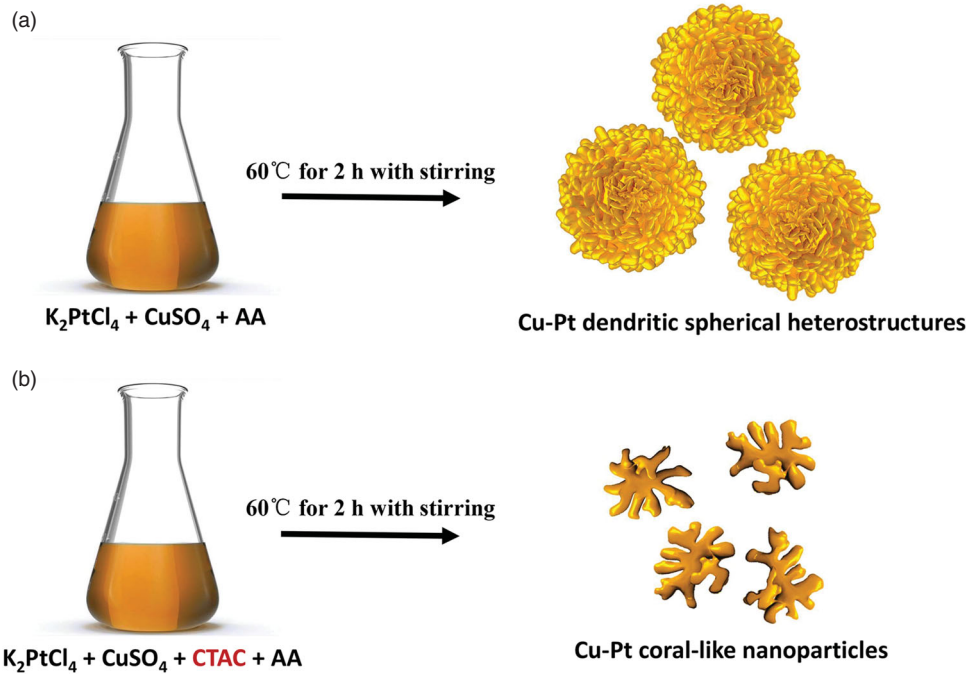

Figure 1. Schematic illustration for the preparation of (a) Cu–Pt dendritic spherical heterostructures without surfactant and (b) Cu–Pt coral-like nanoparticles with CTAC.

solution (5 wt% in lower aliphatic alcohols and water, Sigma-Aldrich), Pt/C (10 wt% Pt, matrix-activated carbon support, Sigma-Aldrich). The ultrapure water with a resistivity of 18.2 MΩ cm is used in the experiment. All the chemicals are used as received without further purification.

Synthesis of Cu–Pt dendritic spherical heterostructures

About 4.5 mL ultrapure water, 0.3 mL of aqueous K_2PtCl_4 (10 mM) and 1 μL of aqueous $CuSO_4$ (1 M) are added in a 10 mL vial in turn. After the mixture is stirred for around 2 min, 0.2 mL of aqueous AA (0.1 M) is added into the mixture rapidly. The resulting homogeneous mixture is transferred into a water bath and heated at 60°C for 2 h with stirring. The products are collected by centrifugation at 12,000 rpm for 10 min, and then washed with ultrapure water and ethanol three times.

Synthesis of Cu–Pt Coral-like Nanoparticles

In a typical synthesis of well-organized Cu–Pt coral-like nanoparticles, 4.4 mL ultrapure water, 0.1 mL of aqueous CTAC (0.1 M), 0.3 mL of aqueous K_2PtCl_4 (10 mM) and 1 μL of aqueous $CuSO_4$ (1 M) are added in a 10 mL vial in turn. After the mixture is stirred for around 2 min, 0.2 mL of aqueous AA (0.1 M) is added into above mixture rapidly. The resulting homogenous mixture is transferred into a water bath and heated at 60°C for 2 h with stirring. The products are collected by centrifugation at 12,000 rpm for 10 min, and then washed with ultrapure water three times.

Instrumentation

X-ray diffraction (XRD) is performed on a Bruker D8 Advance with Cu Kα radiation ($\lambda = 1.54178$ Å). Transmission electron microscopy (TEM) and high-resolution TEM (HR-TEM) images are prepared with the FEI Tecnai G2 F20 S-Twin microscope at an acceleration voltage of 200 kV. The high-angle annular dark-field scanning transmission electron microscopy (HAADF-STEM) images and EDS mapping images are carried out on the FEI Titan3 G2 80–300 microscope at an acceleration voltage of 300 kV. Inductively coupled plasma optimal emission spectrometry (ICP-OES) is used to measure the contents of the Cu–Pt alloy.

Electrochemical measurements

Electrochemical measurements are conducted with a three electrode system on a CHI 660D electrochemical workstation (Shanghai Chenhua Instruments). The working electrode is a glassy-carbon electrode (GCE, CHI104, diameter: 3 mm, area: 0.071 cm^2), a Pt wire is used as the counter electrode, an Ag/AgCl is used as the reference electrode in 3 M KCl solution. The Pt loading of Cu–Pt coral-like nanoparticles, Cu–Pt dendritic spherical heterostructures and Pt/C are all 4 μg. The electrochemical active surface area (ECSA) measurements are determined by integrating the hydrogen adsorption charge on the cyclic voltammetry (CV) at room temperature in argon-saturated 0.5 M H_2SO_4 solution. The potential scan rate is 50 mV/s for the CV measurement. Prior to methanol oxidation measurements, 1.0 M KOH (or 0.1 M $HClO_4$) and 1.0 M CH_3OH are purged with argon for 0.5 h. The scan rate was 50 mV/s. The durability tests are performed at room temperature in 1.0 M KOH (or 0.1 M $HClO_4$) and 1.0 M CH_3OH solutions by applying cyclic potential sweeps between −0.8 and 0.1 V (or 0 and 1.0 V) versus the Ag/AgCl electrode at a sweep rate of 50 mV/s for 1,500 cycles.

Results and discussion

Figure 2(a, b) shows the well-designed Cu–Pt dendritic spherical heterostructures through TEM, and the average size is estimated to be 52.4 ± 4.3 nm. For better understanding the atomic distributions of Cu and Pt in the dendritic heterostructures, the HAADF-STEM and elemental mappings of Cu and Pt atoms distribution are conducted (Figure 2(c–f)). The merged mappings provide clear evidence for the elements distribution, the presence of Cu (green) and Pt (red) appears in the individual bimetallic nanostructure, further illustrating a completely overlapping structure of two elements.

Simultaneously, the achieved Cu–Pt coral-like nanoparticles are characterized by TEM, HAADF-STEM and elemental mapping (Figure S1A†). The overall Cu–Pt coral-like nanoparticles exhibit highly uniform morphology and size of 16.2 ± 2.0 nm. The Cu–Pt coral-like nanoparticle consist of irregular dendritic structures as shown in Figure S1B†, Cu and Pt atoms distribute evenly among each particle (Figure S1D-F†). These coral-like nano-architectures dramatically promote the specific surface area, which result in a slight enhancement of catalytic activity investigated by MOR measurements.

The low-angle XRD is carried out in order to confirm the crystalline structures of Cu–Pt dendritic spherical heterostructures and Cu–Pt coral-like nanoparticles (Figure S2†). The patterns demonstrate that the typical peaks of both nanoparticles can be referenced to a face-centered cubic (*fcc*) structure, corresponding to the pure *fcc* Cu (JCPDS no. 85-1,326) and the pure *fcc* Pt (JCPDS

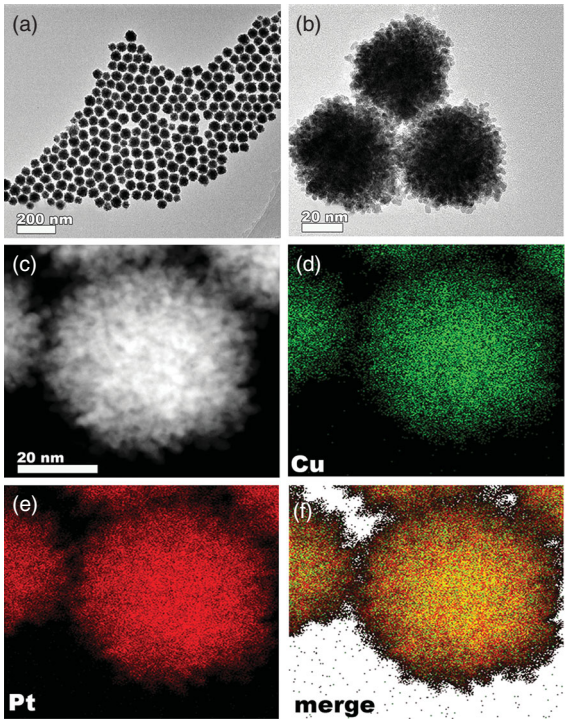

Figure 2. Structural and compositional analysis of the well-designed Cu–Pt dendritic spherical heterostructures. (a, b) Low-magnification TEM and HR-TEM images of Cu–Pt dendritic spherical heterostructures with distinctive uniformity and dispersibility. (c, d–f) High-magnification HAADF-STEM and elemental mapping images of Cu–Pt dendritic spherical heterostructures.

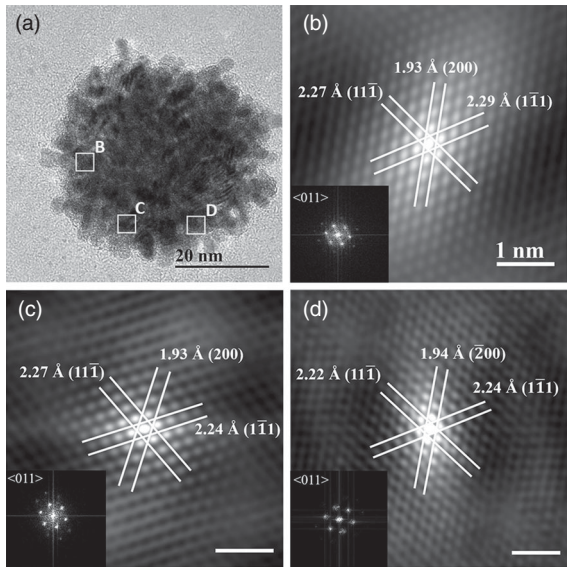

Figure 3. (a) HRTEM image of Cu–Pt dendritic spherical nanostructures, (b)–(d) are the ACF image of region marked by the white box in (a). Insets show the corresponding FFT patterns. The scale bar in (c) and (d) is 1 nm.

no.87–0,646). According to Vegard's law, the Cu–Pt dendritic spherical nanostructures and the Cu–Pt coral-like nanoparticles are estimated as Pt3Cu,[33, 34] which is equal to the ratio of Pt/Cu measured by ICP-OES.

In addition, the individual Cu–Pt dendritic spherical heterostructures and the Cu–Pt coral-like nanoparticles are further characterized by HRTEM (Figure 3, Figure S3†). The auto correlation function (ACF) images and the corresponding fast Fourier transform (FFT) images were observed from the crystal axis [011], which also indicate that Cu–Pt dendritic spherical and Cu–Pt coral-like nanoparticles have fcc structure on their [110]. Through measuring the lattice spacing of two samples we prepared, {200} and {111} planes are observed which are consistent with the observation by XRD on the whole. As confirmed by ACF images and the corresponding FFT pattern, a continuous crystal lattice clearly revealed a good crystallinity for an individual Cu–Pt nanocrystal.

Interestingly, considering all the experimental parameters, it is found that the molar ratio of $K_2PtCl_4/CuSO_4$ is the crucial actor for successful synthesizing of Cu–Pt dendritic spherical heterostructures. Figure S4† illustrates the variations of the Cu–Pt dendritic spherical heterostructures growth by tuning the molar ratios of $K_2PtCl_4/CuSO_4$. As in the cases of the molar ratios of $K_2PtCl_4/CuSO_4$: (9:1), (6:1), (3:1) and (1:1), similar dendritic spherical nanostructures are obtained (Figure S4A-D†). However, as the molar ratio of $K_2PtCl_4/CuSO_4$ is 1:3, thus the Cu–Pt quantum dots with large uniformity and dispersibility are achieved and formed with size of 3 nm averagely (Figure S4E†). In terms of synthesis on the Cu-Pt coral-like nanoparticles, the less volume of Pt precursor used, then the smaller size of Cu-Pt coral-like nanoparticles obtained (Figure S5†). As the molar ratio of $K_2PtCl_4/CuSO_4$ is varied to be 3:1, the obtained Cu–Pt coral-like nanoparticles are in uniform shape and size.

The Cu–Pt dendritic spherical heterostructures and the Cu–Pt coral-like nanoparticles are expected to exhibit enhanced electrochemical activity for MOR. For comparison, commercial Pt/C is investigated in the same condition. The ECSA is evaluated by integrating the charge in the hydrogen desorption region after correction for double layer contribution between −0.3 and 1.0 $V_{Ag/AgCl}$. According to the CV curves shown in Figure 4, the ECSAs is calculated as 41.09 $m^2 g^{-1}$ Pt for the Cu–Pt coral-like nanoparticles, 35.66 $m^2 g^{-1}$ Pt for the Cu–Pt dendritic spherical heterostructures and 67.10 $m^2 g^{-1}$ Pt for the commercial Pt/C. The ECSA of Pt/C is the highest than those of Cu–Pt coral-like nanoparticles and Cu–Pt dendritic spherical heterostructures, due to the Pt nanoparticles with smaller size possessing much higher active surface area. The highly branched structures of Cu–Pt coral-like nanoparticles provide a reasonably higher surface area compared to

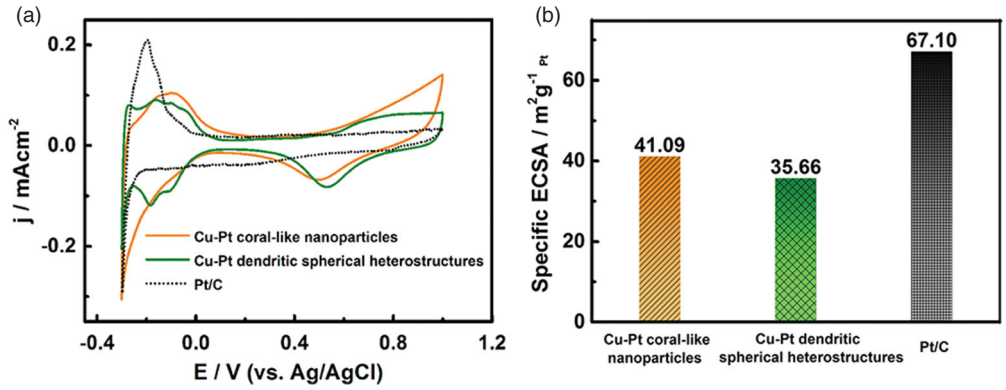

Figure 4. (a) CV of Cu–Pt coral-like nanoparticles, Cu–Pt dendritic spherical heterostructures and commercial Pt/C catalysts recorded at room temperature in Ar_2-purged 0.5 M H_2SO_4 solution with a sweep rate of 50 mV/s. (b) The bar graph of Pt specific ECSA of three catalysts.

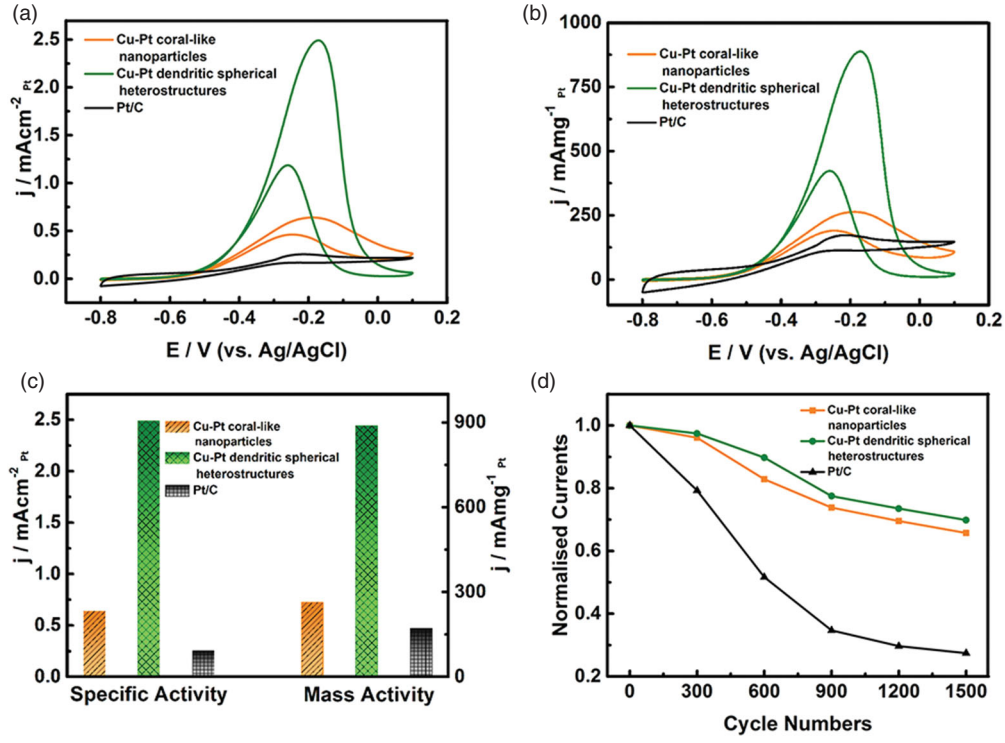

Figure 5. CV of Cu–Pt coral-like nanoparticles, Cu–Pt dendritic spherical heterostructures and commercial Pt/C exhibiting the catalytic activity for methanol oxidation in alkaline conditions. (a) Specific activity and (b) mass activity CV cycles obtained in solutions with 1 M in both KOH and CH_3OH. (c) The bar graph of specific activities and mass activities (at −0.2 vs. Ag/AgCl). (d) The stability of normalized current during 1,500 cycles.

the Cu–Pt dendritic spherical heterostructures with large overall particle size relatively.

The MOR measurements are performed in an Ar_2-purged 1.0 M KOH and 1.0 M CH_3OH solution from −0.8 to 0.1 V at a scan rate of 50 mV s^{-1}. The CVs for specific activities and mass activities of Cu–Pt coral-like, Cu–Pt dendritic spherical heterostructures and commercial Pt/C are investigated, as shown in Figure 5(a–c). The peak current density of Cu–Pt dendritic spherical heterostructures is much higher than that of Cu–Pt coral-like particles and commercial Pt/C. For specific activities, the current density of Cu–Pt dendritic spherical heterostructures (2.49 mA cm^{-2}) is around four times that of Cu–Pt coral-like nanoparticles (0.64 mA cm^{-2}), and 10 times that of Pt/C (0.25 mA cm^{-2}), respectively. Regard to mass activities, it obviously reveals that the function of Cu–Pt dendritic spherical heterostructures is the optimal among three catalysts. Moreover, the catalytic activities illustrate as following: Cu–Pt dendritic spherical heterostructures > Cu–Pt coral-like

nanoparticles > commercial Pt/C, with current–density values of 888.0, 263.2, and 172.3 mA mg^{-1}, respectively.

Furthermore, we evaluate the long-term stability of Cu–Pt dendritic spherical heterostructures, Cu–Pt coral-like nanoparticles and commercial Pt/C catalysts through accelerating durability tests by continuous CV measurements performed from −0.8 to 0.1 V at a scan rate of 50 mV s^{-1} for 1,500 cycles (Figure S6†). As shown in Figure 5(d), it demonstrates that the value of initial forward current density of Cu–Pt dendritic spherical heterostructures and Cu–Pt coral-like nanoparticles still remains 70% and 65% after 1,500 cycles, whereas the commercial Pt/C loses 73% of its initial current density comparably. Additionally, TEM characterizations confirm that most of Cu–Pt heterostructures maintain their dendritic nanospherical morphology after continuous CV evaluation for 1,500 cycles (Figure S7A†), further evidencing the long-term durability. Cu–Pt coral-like nanoparticles partially dissolve and aggregate during the durability investigation (Figure S7B†).

The mechanism of superior catalytic performance for Cu–Pt dendritic spherical heterostructures can be attributed to the typical geometrical morphology and heterostructures. The dendritic Cu–Pt alloys provide plenty of Pt stepped atoms and edge atoms on surface shown by the HRTEM image Figure S8†, which could supply abundant activated sites for methanol oxidation. Simultaneously, the synergistic effect between Cu and Pt caused by lattice strain effects and geometrical variation can dramatically enhance their electrocatalytic functions and durability. Possibly, Pt catalyzes methanol oxidation generating as Pt–CO, while Cu promotes water dissociating as Cu–OH, then Pt–CO and Cu–OH interact to generate CO_2, thus sufficient Pt active sites are released for maintaining continuous MOR. In addition, the efficiency of Cu–Pt electrons transfer is significantly promoted during the fabrication of Cu–Pt dendritic spherical heterostructures without introducing any surfactant. In Cu–Pt coral-like nanoparticles with inferior electrocatalytic activities because it is impossible to wash off the surfactant thoroughly results in the residual CTAC molecules still adsorbed on the surface of nanostructures, which could severely influence their catalytic functions. It should be pointed out that Cu as a supporting element is essential to reduce the amount of Pt particles while maintaining the high catalytic activity.

Meanwhile, we conducted the catalytic efficiency of MOR in acidic environment to compare with those of alkaline media. As shown in Figure S9A–C†, the catalytic properties of Cu–Pt dendritic spherical heterostructures, Cu–Pt coral-like nanoparticles and commercial Pt/C are much lower than those of the alkaline condition. Even though the Cu–Pt dendritic spherical heterostructures exhibit pretty much low value of current density after 1,500 cycles, the value of current density of Cu–Pt coral-like nanoparticles only retain 16.7%. The possible reason caused is that the adsorption strength of the intermediate products in an alkaline solution is much weaker than that of acidic solution, which results in highly enhanced electrocatalytic activity for MOR in former media.

Conclusion

In summary, the well-designed Cu–Pt dendritic spherical heterostructures are synthesized successfully without introducing any surfactants or organic solvents as protective agent, and the Cu–Pt coral-like nanoparticles are prepared using CTAC for comparison. It reveals that the well-designed Cu–Pt dendritic spherical heterostructures exhibit highly enhanced electrocatalytic property and durability toward MOR, compared with the obtained Cu–Pt coral-like nanoparticles and commercial Pt/C. Moreover, the highly promoted electrocatalytic activity and stability can be attributed to these unique dendrite structures of Cu–Pt through the modified synthesis approach. This advanced facile and green synthesis technique could scale up bimetallic heterostructures with high yield, and it provides a concept for fabricating other trimetallic or multimetallic nanoarchitechtures with tunable morphology and size.

Disclosure statement

No potential conflict of interest was reported by the authors.

Funding

The presented research was financially supported by the Natural Science Foundation of China [21401211] and [31571013], Key International S&T Cooperation Project [2015DFH50230], Instrument Developing Project of Chinese Academy of Science [YZ201439], Shenzhen Science and Technology Program [KQCX20140521115045447], the JSPS KAKENHI [26420661] and the 'Nanotechnology Platform' from the Ministry of Education, Culture, Sports, Science and Technology (MEXT), Japan.

References

[1] Stamenkovic VR, Fowler B, Mun BS, et al. Improved oxygen reduction activity on Pt3Ni(111) via increased surface site availability. *Science*. 2007;315(5811):493–497.
[2] Chen ZW, Waje M, Li WZ, Yan YS. Supportless Pt and PtPd nanotubes as electrocatalysts for oxygen-reduction reactions. *Angew Chem Int Edit*. 2007;46(22):4060–4063.
[3] Park J, Zhang L, Choi SI, et al. Atomic layer-by-layer deposition of platinum on palladium octahedra for enhanced

catalysts toward the oxygen reduction reaction. *ACS Nano*. 2015;9(3):2635–2647.
[4] Arico AS, Creti P, Kim H, Mantegna R, Giordano N, Antonucci V. Analysis of the electrochemical characteristics of a direct methanol fuel cell based on a Pt-Ru/C anode catalyst. *J Electro Chem Soc*. 1996;143(12):3950–3959.
[5] Xu D, Liu Z, Yang H, et al. Solution-based evolution and enhanced methanol oxidation activity of monodisperse platinum–copper nanocubes. *Angew Chem*. 2009;121(23):4281–4285.
[6] Lee HJ, Habas SE, Somorjai GA, Yang PD. Localized Pd overgrowth on cubic Pt nanocrystals for enhanced electrocatalytic oxidation of formic acid. *J Am Chem Soc*. 2008;130(16):5406–5407.
[7] Guo SJ, Wang EK. Noble metal nanomaterials: controllable synthesis and application in fuel cells and analytical sensors. *Nano Today*. 2011;6(3):240–264.
[8] Xia BY, Wu HB, Wang X, Lou XW. Highly concave platinum nanoframes with high-index facets and enhanced electrocatalytic properties. *Angew Chem Int Edit*. 2013;52(47):12337–12340.
[9] Wu YE, Wang DS, Li YD. Nanocrystals from solutions: catalysts. *Chem Soc Rev*. 2014;43(7):2112–2124.
[10] Gasteiger HA, Markovic N, Ross PN, Cairns EJ. Co electrooxidation on well-characterized Pt-Ru alloys. *J Phys Chem*. 1994;98(2):617–625.
[11] Mavrikakis M, Hammer B, Norskov JK. Effect of strain on the reactivity of metal surfaces. *Phys Rev Lett*. 1998;81(13):2819–2822.
[12] Schlapka A, Lischka M, Gross A, Kasberger U, Jakob P. Surface strain versus substrate interaction in heteroepitaxial metal layers: Pt on Ru(0001). *Phys Rev Lett*. 2003;91(1):0161011–0161014.
[13] Kitchin JR, Norskov JK, Barteau MA, Chen JG. Role of strain and ligand effects in the modification of the electronic and chemical properties of bimetallic surfaces. *Phys Rev Lett*. 2004;93(15):1568011–1568014.
[14] Gauthier Y, Schmid M, Padovani S, et al. Adsorption sites and ligand effect for CO on an alloy surface: a direct view. *Phys Rev Lett*. 2001;87(3):0361031–0361034.
[15] Wang L, Nemoto Y, Yamauchi Y. Direct synthesis of spatially-controlled Pt-on-Pd bimetallic nanodendrites with superior electrocatalytic activity. *J Am Chem Soc*. 2011;133(25):9674–9677.
[16] Lin ZH, Lin MH, Chang HT. Facile synthesis of catalytically active platinum nanosponges, nanonetworks, and nanodendrites. *Chem Eur J*. 2009;15:4656–4662.
[17] Taylor E, Chen S, Tao J, Wu L, Zhu Y, Chen J. Synthesis of Pt–Cu nanodendrites through controlled reduction kinetics for enhanced methanol electro-oxidation. *ChemSus Chem*. 2013;6(10):1863–1867.
[18] Ahmadi TS, Wang ZL, Green TC, Henglein A, ElSayed MA. Shape-controlled synthesis of colloidal platinum nanoparticles. *Science*. 1996;272(5270):1924–1925.
[19] Chen JY, Herricks T, Geissler M, Xia YN. Single-crystal nanowires of platinum can be synthesized by controlling the reaction rate of a polyol process. *J Am Chem Soc*. 2004;126(35):10854–10855.
[20] Wang C, Daimon H, Onodera T, Koda T, Sun SH. A general approach to the size- and shape-controlled synthesis of platinum nanoparticles and their catalytic reduction of oxygen. *Angew Chem Int Ed*. 2008;47(19):3588–3591.
[21] Song YJ, Yang Y, Medforth CJ, et al. Controlled synthesis of 2-D and 3-D dendritic platinum nanostructures. *J Am Chem Soc*. 2004;126(2):635–645.
[22] Bratlie KM, Lee H, Komvopoulos K, Yang PD, Somorjai GA. Platinum nanoparticle shape effects on benzene hydrogenation selectivity. *Nano Lett*. 2007;7(10):3097–3101.
[23] Song Y, Garcia RM, Dorin RM, et al. Synthesis of platinum nanowire networks using a soft template. *Nano Lett*. 2007;7(12):3650–3655.
[24] Tripkovic AV, Popovic KD, Grgur BN, Blizanac B, Ross PN, Markovic NM. Methanol electrooxidation on supported Pt and PtRu catalysts in acid and alkaline solutions. *Electrochim Acta*. 2002;47(22–23):3707–3714.
[25] Bock C, Paquet C, Couillard M, Botton GA, MacDougall BR. Size-selected synthesis of PtRu nano-catalysts: reaction and size control mechanism. *J Am Chem Soc*. 2004;126(25):8028–8037.
[26] Xia BY, Wu HB, Li N, Yan Y, Lou XW, Wang X. One-pot synthesis of Pt-Co alloy nanowire assemblies with tunable composition and enhanced electrocatalytic properties. *Angew Chem*. 2015;54(12):3797–3801.
[27] Liu X, Wang W, Li H, et al. One-pot protocol for bimetallic Pt/Cu hexapod concave nanocrystals with enhanced electrocatalytic activity. *Sci Rep*. 2013;3:14011–14015.
[28] Chen S, Su H, Wang Y, Wu W, Zeng J. Size-controlled synthesis of platinum-copper hierarchical trigonal bipyramid nanoframes. *Angew Chem*. 2015;54(1):108–113.
[29] Lim B, Jiang MJ, Camargo PHC, et al. Pd-Pt Bimetallic nanodendrites with high activity for oxygen reduction. *Science*. 2009;324(5932):1302–1305.
[30] Xie X, Gao G, Kang S, et al. Site-selective trimetallic heterogeneous nanostructures for enhanced electrocatalytic performance. *Adv Mater*. 2015;27(37):5573–5577.
[31] Niu ZQ, Li YD. Removal and utilization of capping agents in nanocatalysis. *Chem Mat*. 2014;26(1):72–83.
[32] Duan H, Wang D, Li Y. Green chemistry for nanoparticle synthesis. *Chem Soc Rev*. 2015;44(16):5778–5792.
[33] Best RJ, Russell WW. Nickel, copper and come of their alloys as catalysts for ethylene hydrogenation. *J Am Chem Soc*. 1954;76(3):838–842.
[34] Xiong YJ, McLellan JM, Chen JY, Yin YD, Li ZY, Xia YN. Kinetically controlled synthesis of triangular and hexagonal nanoplates of palladium and their SPR/SERS properties. *J Am Chem Soc*. 2005;127(48):17118–17127.